Epigenetic Adaptation Drives Monocyte Differentiation into Microglia-Like Cells Upon Engraftment into the Central Nervous System

Jie Liu[a*], Fengyang Lei[a*], Bin Yan[a,b] , Tian Cao[a], Naiwen Cui[c], Jyoti Sharma[a], Victor Correa[a], Lara Roach[d], Savvas Nicolaou[a], Kristen Pitts[a], James Chodosh[e], Daniel E. Maidana[f], Demetrios Vavvas[a], Milica A Margeta[a], Huidan Zhang[c], David Weitz[c], Raul Mostoslavsky[d], and Eleftherios I. Paschalis[a]

a. Department of Ophthalmology, Massachusetts Eye and Ear, Harvard Medical School, Boston, MA 02114, USA
b. Department of Ophthalmology, The Second Xiangya Hospital of Central South University, 139 Middle Renmin Road, Changsha, Hunan, 410011, China
c. School of Engineering and Applied Sciences (SEAS), Harvard University, Cambridge, MA, USA.
d. Center for Regenerative Medicine, Massachusetts General Hospital, Harvard Medical School, Boston, MA 02114, USA
e. Department of Ophthalmology and Visual Sciences, University of New Mexico School of Medicine, Albuquerque, NM 87131, USA
f. Department of Ophthalmology and Visual Sciences, Illinois Eye and Ear Infirmary, University of Illinois at Chicago, Chicago, IL

*Equal contribution

Corresponding author: Eleftherios I. Paschalis, eleftherios_paschalis@meei.harvard.edu

Author Contributions: J.L. and E.I.P. designed research; J.L., F.L., N.C. and B.Y. performed research; J.L., F.L., N.C., S.N. and J.S.,V.C., S.N., D.V., D.W., R.M. and M.A.M. analyzed data; and J.L., B.Y., J.C., D.E.M., D.V., D.W., R.M. and E.I.P. wrote the paper.

Competing Interest Statement: The authors declare no competing interest.
Classification: Biological, Health, and Medical Sciences/Immunology and Inflammation, Biological Sciences/Neuroscience.
Keywords: microglia, marker, macrophages, monocytes, CNS, retina, single cell RNAseq, ATAC-seq

This file includes:
Main Text
Figures 1 to 6 and S1 to 4
Tables 1

Abstract

The identification of specific markers to distinguish resident microglia from infiltrating monocytes has been a long-standing challenge in neuroscience. Recently, proteins such as P2RY12, TMEM119, and FCRLS have been proposed as microglia-specific and are now widely used to define microglial populations in health and disease. The specificity of these markers was predicated on the assumption that circulating monocytes retain their distinct signatures after entering the central nervous system (CNS). Here, we challenge this paradigm. Using a combination of bone marrow chimeras, single-cell RNA sequencing, ATAC-seq, flow cytometry, and immunohistochemistry, we demonstrate that monocytes engrafting into the CNS acquire de novo expression of these established microglia markers. This phenotypic conversion is driven by profound epigenetic reprogramming, characterized by dynamic changes in chromatin accessibility at key gene loci, including P2ry12, Tmem119, and Aif1 (Iba1), and a shift in transcription factor binding motifs toward a microglial profile. We show this process occurs in the retina following injury and, remarkably, under physiological conditions in the brain and spinal cord, where blood-derived monocytes progressively contribute to the resident myeloid pool. Furthermore, engrafted monocytes downregulate canonical monocyte markers (Ly6C, CD45), eventually becoming indistinguishable from embryonic microglia based on conventional phenotyping. Our findings reveal that infiltrating monocytes undergo extensive epigenetic and transcriptional remodeling to adopt a microglia-like fate, challenging the specificity of current markers and necessitating a re-evaluation of the distinct roles of these two cell populations in CNS pathology.

Significance Statement

Distinguishing resident CNS microglia from infiltrating monocytes is fundamental to understanding neuro-inflammation. This study reveals that widely used "microglia-specific" markers are not exclusive, as monocytes entering the central nervous system are epigenetically reprogrammed to express them. This mimicry invalidates long-held assumptions about microglial identity and demonstrates that many cells previously identified as microglia may have a peripheral origin. Our work underscores the critical need for more reliable methods to differentiate these populations to accurately define their respective contributions to CNS health and disease.

Introduction

Microglia and infiltrating peripheral monocytes are central players in the pathology of central nervous system (CNS) diseases and have emerged as key therapeutic targets [1-5]. However, given their overlapping functions and morphology, distinguishing these two myeloid populations is notoriously difficult. The use of inadequately specific markers often leads to inadvertent mislabeling, compromising the interpretation of experimental data and our understanding of neuro-inflammatory processes.

Recently, a new panel of markers, including P2RY12, TMEM119, and FCRLS, was proposed to be exclusively expressed by microglia and has been widely adopted[6, 7]. The presumed specificity of these markers was based on comparing CNS-resident microglia with non-CNS monocytes or purified acute immune cells of the CNS [6, 7]. This framework, however, largely overlooked the possibility that monocytes might alter their identity after permanently integrating into the CNS parenchyma. Indeed, recent findings indicate that infiltrating monocytes undergo persistent phenotypic changes upon engraftment, adopting a ramified, microglia-like morphology while retaining a distinct, pro-inflammatory capacity that can drive disease [2, 8].

Here, we hypothesized that peripheral monocytes undergo profound epigenetic reprogramming upon CNS engraftment, enabling them to express canonical microglia markers and confounding their identification. We investigated this hypothesis in the retina—a well-established model of the CNS—and extended our findings to the brain and spinal cord. We demonstrate that shortly after engraftment, monocytes initiate expression of P2RY12, TMEM119, and FCRLS. This phenotypic switch is underpinned by dynamic changes in chromatin accessibility and the acquisition of a microglia-associated transcriptional network, including key transcription factors like PU.1, IRF2, and CEBP. Concurrently, these cells suppress canonical monocyte markers (CCR2, Ly6C, CD45), eventually becoming phenotypically indistinguishable from embryonic microglia by conventional methods.

Our study highlights the remarkable plasticity of monocytes and reveals a fundamental flaw in the tools currently used to identify them. We further demonstrate that the rules governing monocyte engraftment differ across CNS compartments; while injury is required for retinal infiltration, monocytes physiologically populate the brain and spinal cord over time. These findings raise a critical scientific question: how can we reliably discriminate between embryonic microglia and these newly identified monocyte-derived "microglia-like" cells? Answering this is essential to finally untangle the distinct roles of these two crucial immune populations in CNS pathology.

Results

Single-cell RNAseq reveals a transcriptional shift of engrafted monocytes towards a microglia signature

To track the transcriptional fate of myeloid cells after injury, we performed single-cell RNA-seq on isolated CD45+CD11b+ cells from mouse retinas at baseline and at 1, 4, and 7 days after a corneal alkali injury, a model known to induce monocyte infiltration and engraftment [2, 9, 10]. We identified four distinct cell clusters **(Fig. 1A)**. The baseline cluster (Cluster 1) corresponds to native, yolk-sac-derived microglia, as the healthy retina is not populated by peripheral monocytes[2, 8]. By day 1 post-injury, two separate clusters emerged: a monocyte cluster (Cluster 3), identified by high expression of the monocyte marker Siglec1, and a microglia cluster (Cluster 4) with low Siglec1 expression **(Fig. 1B)**

[11]. Remarkably, by day 4, these populations merged into a single transcriptional cluster (Cluster 2), and by day 7, all cells resolved into the original naive microglia cluster (Cluster 1), demonstrating a dynamic transcriptional convergence towards a microglia signature **(Fig. 1A)**.

Gene expression analysis showed that the classical macrophage marker *Cx3cr1* was uniformly expressed, while the monocyte marker *Ccr2* was predominantly expressed in the monocyte-rich cluster 3 (day 1) and the mixed cluster 2 (day 4) **(Fig. 1C, D)**. Critically, the putative microglia markers *p2ry12*, *tmem119*, and *fcrls* were acquired by the engrafting population over time. While *tmem119* and *fcrls* were expressed broadly, *p2ry12* expression was absent in early infiltrating monocytes (day 1) but became highly expressed by day 4 and 7, mirroring the pattern of naive microglia **(Fig. 1C, D)**. *Aif1* (or *iba1*) was expressed in all clusters and highly in cluster 2 (day 4). *P2ry12* expression exhibited temporal regulation in monocytes, with lack of expression in clusters 3 and 4 – both representing early-stage infiltration (Day 1), confirmed in protein studies **(Fig. 1 C, D)**. Using a $CX3CR1^{+/EGFP}$::$CCR2^{+/RFP}$ bone marrow chimera (BMT) model [2, 4, 12], we confirmed via flow cytometry that infiltrating monocytes gradually downregulate their CD45 expression, and by day 7, their CD45 profile becomes indistinguishable from that of resident microglia, further corroborating the scRNAseq findings of a converging cellular signature (Fig. 1E). The BMT model had high transplantation efficiency with of 93.6% of the blood $CD45^{+}CD11b^{+}CX3CR1^{+}$ cells from recipient mice being $EGFP^{+}RFP^{+}$ **(Fig. S1)**. The expected profile of CD45 expression of embryonic microglia was assessed using a transgenic $CX3CR1^{+/EGFP}$ mouse without injury.

By day seven post-injury, flow cytometry confirmed that engrafted CX3CR1+ monocytes modulated their CD45 expression to levels indistinguishable from resident microglia, corroborating the scRNA-seq data indicating a converging cellular signature **(Fig. 1E).** We further validated these transcriptional changes using qPCR on sorted cells from bone marrow chimeras 45 days after engraftment. This analysis confirmed that engrafted monocytes acquire mRNA for *p2ry12*, *tmem119*, *fcrls*, and *aif1* (*Iba1*). Notably, while *p2ry12* mRNA in engrafted monocytes was significantly upregulated compared to blood monocytes, its expression remained lower than that of either naïve or injured microglia. In contrast, resident microglia maintained consistently high expression of these markers in both naïve and injured conditions **(Fig. S2)**.

Engrafted monocytes acquire de novo protein expression of P2RY12, FCRLS, and TMEM119

We next sought to confirm if these transcriptional changes translate to the protein level. Using $CX3CR1^{+/EGFP}$::$CCR2^{+/RFP}$ bone marrow chimeras to distinguish donor monocytes (GFP+) from resident microglia (GFP-), we analyzed protein expression in the retina at multiple time points after injury **(Fig. 2A)**. We first verified that circulating blood monocytes lack P2RY12, TMEM119, and IBA1 protein expression **(Fig. S3)**. We also established the protein expression baseline for circulating monocytes prior to CNS engraftment. Flow cytometry analysis of CD45+CD11b+CX3CR1+ blood cells from naïve mice confirmed the absence of FCRLS protein **(Fig. 2D)** and the robust MHC-II protein expression, which served as a positive staining control **(Fig. S3)**.

Following retinal infiltration, engrafted monocytes (EGFP+) began to express these markers. P2RY12 protein was absent at days 1 and 7 (white arrow) but became detectable by day 14 **(Fig. S4)** and was expressed in approximately 55% of engrafted monocytes by day 45, which by then had adopted a ramified, microglia-like morphology **(Fig. 2B, Fig. S4)**. This heterogeneous expression was sustained long-term, at 16 months post-engraftment, as assessed in a $CX3CR1^{CreER-EYFP}$::$ROSA26^{tdTomato}$ bone marrow chimera model **(Fig. S5 A, B)**, while being consistently below the

expression from embryonic microglia. In contrast, TMEM119 expression was rapidly acquired, with 25% of monocytes positive at day 1 and 100% positive by day 7, an expression level that was maintained at 45 days and 16 months **(Fig. 2C, Fig. S5 C)**. Meanwhile, EGFP^{-} embryonic microglia (yellow arrow) displayed robust expression of P2RY12 and TMEM119 protein throughout the study period **(Fig 2 B, C)**.

FCRLS expression was assessed by flow cytometry in CX3CR1$^{+/EGFP}$::CCR2$^{+/RFP}$ bone marrow chimeras. To distinguish cell populations, CX3CR1+ cells were labeled with an anti-CX3CR1 (PE-Cy7) antibody, defining embryonic microglia as PE-Cy7+GFP- and infiltrating monocytes as PE-Cy7+GFP+ **(Fig. S6 A).** The full representative gating strategy is detailed in **Figure S6 B**. A Fluorescence Minus One (FMO) control was used to validate the specificity of the FCRLS staining. FCRLS, was absent on blood monocytes (grey) [7], but was robustly expressed by infiltrating monocytes (purple) as early as day 1 post-injury, at levels even higher than baseline microglia. This expression was sustained and eventually normalized to microglia levels by day 45 **(Fig. 2D, E).** Finally, the pan-myeloid marker IBA1 was expressed by 85% of infiltrating monocytes at day 1 (white arrow) and 100% thereafter **(Fig. S7)**. Embryonic microglia (yellow arrow) also had robust expression of IBA1 throughout the study period **(Fig. S7)**.

These findings were not specific to the injury model, as a chemically-induced retinal injury (NaIO3) that damages the retinal pigment epithelium (RPE) [13] resulted in almost complete depletion of embryonic microglia, subsequent repopulation by peripheral monocytes that uniformly expressed P2RY12, TMEM119, and IBA1 **(Fig. S8)**. This expression was sustained at 3 months, at which point cells have become ameboid, with ~50% of them expressing MHC-II **(Fig. S8)**.

This phenomenon was not restricted to the retina. In healthy, uninjured chimera mice, we observed that peripheral monocytes physiologically infiltrate and engraft into the brain and spinal cord over time. Within one month, these engrafted cells expressed TMEM119 and IBA1, and by one year, they robustly expressed P2RY12 as well, all while maintaining a quiescent, non-inflammatory (MHC-II negative) state and a ramified morphology indistinguishable from resident microglia **(Fig. S9, S10)**.

Chromatin accessibility changes underpin the monocyte-to-microglia phenotypic switch

To investigate the epigenetic basis of this transformation [14-16], we performed ATAC-seq on flow-sorted circulating monocytes, naive microglia, and engrafted monocytes. We found that upon engraftment, monocytes undergo significant changes in chromatin accessibility that mirror those of resident microglia **(Fig. 3)**. For the *p2ry12* and *tmem119* genes, specific chromatin peaks that were present in microglia but absent in circulating monocytes were gained by monocytes after they engrafted into the retina **(Fig. 3B, D)**. For *fcrls* and *aif1* (IBA1), chromatin was already accessible in circulating monocytes, suggesting these genes are epigenetically poised for rapid activation upon receiving the appropriate CNS signals **(Fig. 3C, E)**.

A heatmap of all differential chromatin accessibility peaks clearly shows that engrafted monocytes at day 7 and 45 cluster epigenetically similar to microglia, rather than to their circulating precursors **(Fig. 3F)**. Motif analysis of these differential peaks revealed a dramatic shift in the landscape of accessible transcription factor binding sites. Engrafted monocytes gained enrichment for motifs of hallmark microglia[17] transcription factors, including PU.1, CTCF, IRF, RUNX, and AP-1. Furthermore, they acquired motifs for disease-associated factors [18] like MITF and the pro-inflammatory factor NFKB1, which were not enriched in naive microglia, hinting at a distinct functional potential despite their morphological and marker-based resemblance **(Fig. 4)**. Engrafted monocytes had enriched MAF and

MEF motifs, absent in embryonic microglia. Microglia newly identified motifs in this study STAT1, FOXN1, KLFs, ATF3, and Npas4, were also enriched in engrafted monocytes **(Fig. 4),** suggesting a dynamic open chromatin accessibility shift in monocytes upon engraftment into the retina.

Engrafted Monocytes Downregulate Canonical Markers Ly6C and CD45

To evaluate the stability of canonical monocyte markers during chronic CNS pathology, we tracked the expression of Ly6C and CD45. It is well-established that Ly6C+ monocytes are recruited to the CNS during inflammation [7, 19]., and that microglia can often be distinguished from monocytes based on their intermediate (CD45int) versus high (CD45high) expression of CD45 [20].

Using a $CX3CR1^{+/EGFP}$::$CCR2^{+/RFP}$ bone marrow chimera model, we followed the phenotypic evolution of monocytes after engraftment into the retina **(Fig. 5A)**. We observed a clear transition over 45 days: infiltrating monocytes, which were initially $CCR2^{high}CX3CR1^{low}$ (Group 1), progressively matured into a predominantly $CCR2^{low/-}CX3CR1^{high}$ population (Group 5), becoming phenotypically similar to resident microglia (Group 6) **(Fig. 5B)**.

Ly6C expression was tightly coupled to this transition. Early infiltrating $CCR2^{high}$ monocytes displayed high levels of Ly6C, which was then gradually downregulated as the majority of cells adopted the $CCR2^{low/-}CX3CR1^{high}$ engrafted phenotype (Group 5) **(Fig. 5C, D)**. Notably, a small subpopulation of engrafted monocytes that retained high CCR2 expression also maintained high Ly6C levels throughout the study period (Group 4) **(Fig. 5C, D)**.

The expression of CD45 followed a similar pattern of repression. While the distinction between CD45high monocytes and CD45int microglia was clear at day 1 and 7, the majority of engrafted monocytes (88.5% of GFP+ cells) downregulated CD45 to intermediate levels by day 45, blurring the distinction between the two cell types **(Fig. 5E-G)**.

Collectively, these data demonstrate that in a chronic setting, the expression of both Ly6C and CD45 on engrafted monocytes converges with that of resident microglia. This renders these conventional markers unreliable for accurately discriminating between the two populations long-term. A comprehensive summary of these dynamic changes in morphology and marker expression over time is provided in **Figure 6**.

Discussion

The precise contribution of microglia to CNS pathology remains a subject of intense debate, with studies reporting both neuroprotective and deleterious roles [21-25]. This controversy is fueled by technical limitations and, as our study demonstrates, a critical lack of specific markers to differentiate resident microglia from peripherally-derived monocytes that infiltrate and permanently engraft into the CNS [2]. Here, we provide definitive evidence that engrafted monocytes are epigenetically reprogrammed to express a suite of markers—P2RY12, TMEM119, FCRLS, and Iba1—that are widely considered to be microglia-specific. This finding challenges the foundations of how these cell populations are identified and calls for a re-evaluation of their respective roles in CNS disease, in light of the more pro-inflammatory phenotype of monocytes [2, 26].

Our data directly refute the presumed specificity of TMEM119 and P2RY12. While TMEM119 was proposed as a stable marker to differentiate microglia from infiltrating monocytes [6], we show that CCR2+ monocytes begin expressing TMEM119 within a day of retinal infiltration, with ubiquitous expression in engrafted cells thereafter. Similarly, P2RY12 and FCRLS, which were initially characterized as absent from infiltrating monocytes in acute EAE models [7], are clearly upregulated in our chronic engraftment models across the retina, brain, and spinal cord. The expression of P2RY12 was notably heterogeneous and appeared later, suggesting a more complex and gradual maturation process. This dynamic and region-specific regulation was particularly evident in the spinal cord, where P2RY12 expression was absent in engrafted cells at one month but became robust by one year.

These findings have profound implications. For instance, in Alzheimer's disease research, P2RY12-negative myeloid cells surrounding Aβ plaques are often interpreted as dysfunctional microglia contributing to pathology [27, 28]. Our results raise the provocative possibility that this P2RY12-negative population could, in fact, be composed of recently engrafted monocytes. If true, this would fundamentally alter the interpretation of their role, shifting the focus from microglial failure to the pathological contribution of a distinct, peripherally-derived cell type. Likewise, the ubiquitous use of IBA1 [28-35] and CD45 [36] expression profiles to identify microglia in studies of tauopathy and multiple sclerosis must be reconsidered, as we show that long-term engrafted monocytes adopt an IBA1+ and $CD45^{int}$ signature identical to that of resident microglia. Lastly, the use of expression of $CD45^{hi}$ $CD11b^{+}$ conventional marker is also inadequate, as engrafted monocytes have similar expression levels ($CD45^{lo}$ $CD11b^{+}$) at 45 days as microglia.

Mechanistically, our work reveals that this phenotypic convergence is driven by deep epigenetic remodeling. The ATAC-seq analysis provides a compelling explanation for the observed changes, showing that engrafted monocytes gain chromatin accessibility at key microglia identity gene loci (*P2ry12, Tmem119*). The motif analysis further solidifies this conclusion, revealing an enrichment for transcription factors like PU.1, IRF, and RUNX, which are known master regulators of microglial identity and microgliogenesis in humans and mice [17, 37]**.** Other established microglia genes, such as SPP1, C1qa, and Ms4a7 [38] also become accessible after monocyte engraftment, a feature not observed in circulating blood monocytes. Critically, this analysis also provides a mechanistic clue to the functional divergence of these cells. The unique enrichment of motifs for the disease-associated transcription factor MITF and the pro-inflammatory hub NFKB1 in engrafted monocytes—but not in naive microglia—offers a powerful molecular explanation for their previously reported pro-neurodegenerative phenotype [2, 18]. Thus, while they acquire the *look* of microglia, they appear epigenetically hardwired for a more aggressive, inflammatory response.

We also uncover a fundamental difference in immune surveillance across the CNS. In healthy animals, monocyte engraftment is a normal physiological process in the brain and spinal cord as shown in the current study, occurring steadily over the animal's lifespan, as well as the optic nerve as shown by our laboratory previously [2, 4]. In contrast, the healthy retina remains exclusively populated by embryonic microglia, requiring injury to trigger monocyte infiltration [2]. This distinction has major implications for understanding regional vulnerability and designing region-specific therapies. The state of cellular activation may be more critical than ontology; quiescent monocytes replacing microglia in the healthy brain are MHC-II negative, whereas injury-elicited monocytes in the retina are MHC-II positive and reactive **(Fig. S8).** This suggests that targeting the *function* of reactive monocytes, perhaps via epigenetic modulation, could be a powerful therapeutic strategy. This study has limitations. The bone marrow chimera model relies on myeloablation, which could potentially alter hematopoiesis, though we achieved near-complete chimerism with minimal barrier disruption [2]. Parabiosis models could offer an alternative, though more technically challenging to establish [39]. Cre-based fluorescent lineage tracing model could also be an alternative [8, 40], but incomplete activation or leaky Cre expression can lead to mislabeling of microglia and monocytes. Our model achieved near complete chimerism (~95%) and long-term engraftment of the donor cells into the CNS, which is essential for molecular profiling. While we provide robust ATAC-seq data, future studies using CUT&RUN [41] or ChIP-seq [17] could further dissect the specific histone modifications and enhancer landscapes driving this transformation. Future studies will need to investigate the functional dichotomy of these long term CNS engrafted monocytes and their ability to present as homeostatic microglia while primed for hyperinflammation. This potential hybrid state could explain the clinical difficulty of chronic neurodegenerative diseases.

In conclusion, our study demonstrates that the CNS microenvironment actively reshapes the identity of infiltrating monocytes, compelling them to adopt a microglia-like phenotype and express canonical microglia-specific markers. This mimicry invalidates their use for definitive lineage tracing in chronic disease settings. Until truly stable and specific protein markers are developed, the field must rely on sophisticated fate-mapping strategies and remain vigilant about the potential for cellular misidentification. Unraveling the functional consequences of this remarkable cellular plasticity will be key to understanding and ultimately treating a wide range of debilitating CNS diseases.

Materials and Methods

Animal Models and Procedures:

All animal experiments were conducted in strict accordance with the Association for Research in Vision and Ophthalmology (ARVO) Statement for the Use of Animals in Ophthalmic and Vision Research and were approved by the Animal Care Committee of the Massachusetts Eye and Ear. Mice were bred and housed at the Massachusetts Eye and Ear Animal Facility and were used at 6–12 weeks of age.

Bone-Marrow Chimera Generation:

To distinguish resident microglia from infiltrating peripheral monocytes, we generated bone marrow transplant (BMT) chimeras. Briefly, recipient C57BL/6J mice were myelodepleted via intraperitoneal (i.p.) injections of busulfan (35 mg/kg; Sigma-Aldrich) administered 7, 5, and 3 days prior to transplantation. Bone marrow cells (5 x 10^6) were harvested from donor mice (either $CX3CR1^{+/EGFP}$::$CCR2^{+/RFP}$ or $CX3CR1^{+/EGFP}$ or $CX3CR1^{CreER\text{-}EYFP}$::$ROSA26^{tdTomato}$) and transferred into

275 the myelodepleted recipients via tail vein injection one month before experimental injury. To prevent
276 infection, mice received Bactrim (trimethoprim/sulfamethoxazole) in their drinking water for 15 days
277 following busulfan treatment.Recipient C57BL/6J (Stock No. 000664), Ccr2-RFP (Stock No. 017586),
278 CX3CR1-EGFP (Stock No. 005582), Cx3cr1-CreER (Stock No. 021160), and ROSA26-tdTomato
279 (Stock No. 007914) mice were obtained from The Jackson Laboratory. CX3CR1+/EGFP::CCR2+/RFP
280 donor mice were generated by crossing Ccr2-RFP and CX3CR1-EGFP lines
281
282 **Tamoxifen administration:**
283 For lineage tracing in the CX3CR1$^{CreER\text{-}EYFP}$::ROSA26^{tdTomato} chimera model, tamoxifen (20 mg/ml in
284 corn oil) was administered two weeks after corneal injury, a time point allowing for monocyte infiltration
285 and engraftment. Mice received two i.p. injections of tamoxifen at a dosage of 75 mg/kg, separated by
286 one day, as previously described [42].
287
288 **Mouse Model of Alkali Burn:**
289 One month after BMT, corneal alkali burns were induced as previously described. Briefly, mice were
290 anesthetized with ketamine (60 mg/kg) and xylazine (6 mg/kg). Following application of topical
291 proparacaine, a 2-mm filter paper soaked in 1 M NaOH was applied to the cornea for 20 seconds. The
292 eye was immediately irrigated with sterile saline for 15 minutes. For post-procedural analgesia, Ethiqa
293 XR (buprenorphine, 3.25 mg/kg,(Covetrus North America, Cat: FP-001) was administered
294 subcutaneously, and topical Polytrim antibiotic (polymyxin B/trimethoprim; Bausch & Lomb, Inc.) was
295 applied to the eye.
296
297 **NaIO3 injury model:**
298 Retinal injury was also induced by a single i.p. injection of $NaIO_3$ (30 mg/kg; Sigma-Aldrich, Cat.
299 S4007), per an established protocol. Animals were euthanized 14 days post-injection for analysis.
300
301 **Flow Cytometry and Cell Sorting**:
302 Flow cytometry was used to analyze FCRLS, Ly6C, and CD45 expression and to sort cells for scRNA-
303 seq and ATAC-seq. Retinas were collected from CX3CR1$^{+/GFP}$::CCR2$^{+/RFP}$ chimeras at 1 day, 7 days,
304 and 1.5 months post-injury and digested into single-cell suspensions using papain (Worthington
305 Biochemical Corporation, Cat: LK003150). Infiltrating monocytes were identified as
306 CD45+CD11b+GFP+ cells, while resident microglia were identified as CD45+CD11b+CX3CR1+GFP-
307 cells. After blocking with anti-CD16/32 (clone: 2.4G2), cells were stained with primary antibodies
308 (Table 1) and analyzed on a BD FACSAria™ III cell sorter using FlowJo™ 10 software.
309
310 **Single cell RNAseq and gene expression profiling:**
311 Flow-sorted CD45+CD11b+ cells were encapsulated in microdroplets for single-cell library
312 preparation. Using a high-throughput microfluidic platform, barcoded hydrogel beads containing
313 reverse transcription reagents were picoinjected into the droplets to initiate in-drop cDNA
314 synthesis. Libraries were prepared according to Klein et al. and sequenced on an Illumina HiSeq 2500
315 (100 bp paired-end) with approximately 1,000 cells per sample. Reads were mapped and quantified,
316 and gene counts were normalized to reads per million (RPM).
317
318 **RNA isolation and Quantitative real-time PCR analysis**

A bone marrow transfer model was used to distinguish periphery infiltrated monocyte and resident microglia. Naïve microglia cells and blood monocyte were collected from uninjured bone marrow transferred mice. Injured microglia and engrafted monocyte were collected from retinas 45 days after ocular injury in bone marrow transferred mice. Cells were directly collected into 1ml Trizol (Thermo Fisher, Cat: 15596026). RNA extraction was performed per standard assay recommendations Specifically, GlycoBlueTM Coprecipitant (Thermo Fisher,Cat: AM9515) was added in the RNA precipitation step to help visualize the RNA pellet. SMART-Seq V4 Ultra Low Input RNA Kit (Takara, Cat: 634890) was employed for RNA reverse transcription and cDNA amplification. RNA from around 400 cells was loaded in the experiment and 30ng cDNA could be yield after 18 cycles of cDNA amplification. cDNA amount was measured with Qubit dsDNA Quantification Assay kit (High sensitivity) (Thermo Fisher, Cat: Q32851). Quantitative real-time PCR analysis was conducted using TaqMan Probes and TaqMan universal PCR Master Mix (Thermo Fisher, Cat: 4304437). 250pg-500 pg cDNA was loaded for each PCR reaction.

ATAC-seq

The $CX3CR1^{+/EGFP}$::$CCR2^{+/RFP}$ bone marrow transfer model was used to distinguish peripheral infiltrated monocyte and resident microglia. For flow sorting, infiltrated monocytes were gated as $CD45^{+}CD11b^{+}GFP^{+}$ cells and microglia as $CD45^{+}CD11b^{+}CX3CR1^{+}GFP^{-}$. Each sample was pooled from 5 retinas (from 5 mice) and 1000 to 5000 cells collected and used for ATAC-seq analysis with the ATAC-seq kit from Active motif (Cat: 13150). Briefly, nuclei were isolated by adding 100 µL ice cold ATAC-lysis buffer and then incubated with the tagmentation master mix in a shaking heat block at 37°C/800 rpm for 30 min. Obtained DNA was purified and library generated by PCR reaction for 13 cycles using indexed primers according to the manufacturer's instructions. A quality control (QC) was performed to verify the size distribution of the PCR enriched library fragments. ATAC-seq sequencing was performed on an Illumina HiSeq 2000 instrument, resulting in 30 million paired-end 50 bp reads per sample. Reads were mapped to the mm9 reference mouse genome using BWA [43]. Those fragments with both ends unambiguously mapped to the genome that were longer than 100 bp were used for further analysis. Hotspot2 was used to detect significant peaks with FDR cutoff of 0.05 [44]. For the analysis of overlap between peak regions, we used a cutoff of 50% reciprocal overlap between the two compared regions. For the analysis of differential chromatin accessibility between groups of replicate samples, DiffBind R package was used: (https://bioconductor.riken.jp/packages/3.2/bioc/vignettes/DiffBind/inst/doc/DiffBind.pdf). Motif analysis was performed through MEME-CHIP (motif analysis of large nucleotide datasets).

Immunohistochemistry and Imaging

Mouse retinas were collected and prepared for flat mount staining 1, 7 and 45 days and 16 months after corneal alkali injury. Eyes were fixed in 4% paraformaldehyde overnight at 4°C then dissected. Mouse brain and spinal cord tissues were fixed in 4% paraformaldehyde overnight at 4°C and sections at 12 *µm* thickness. Immunostaining was performed by first blocking with PBS containing 5% normal donkey serum, 0.25% Triton-X-100 for 1 hour at room temperature, following by incubation of the tissues with primary antibody overnight or over the weekend at 4°C, and subsequent staining with secondary antibody, (**Table 1)**. For retinal flat-mounts, whole retinas were laid flat after performing radial relaxing incisions and mounted on glass slides with coverslip. Images were captured using the Axio imager M2 (M2, Zeiss, Oberkochen, Germany).

363
364 **Statistics**
365 Results were analyzed with Prism 9 software. Medium fluorescence intensity (MFI) was used for
366 quantification in flow cytometry experiments. Normality of data was assessed using the Shapio-Wilk
367 test (less than 50 samples) and independent Student's t test (unpaired, nonparametric or parametric
368 depends on data type) was used to assess statistical significances between groups. Significance was
369 assumed for $P < 0.05$.
370
371 **Acknowledgments**
372 This work was supported by the Boston Keratoprosthesis Research Fund, Department of Defense
373 (W81XWH2210774, W81XWH2010916), National Institute of Health (7R01EY013124,
374 5P30EY003790), and the Retina Research Foundation (RRF).
375

Figure Legends

Figure 1. Single-cell RNAseq analysis for retinal CD45$^+$CD11b$^+$ cells 0, 1, 4 and 7 days after ocular injury.

(A) Principal component analysis shows the existence of 4 clusters with distinct transcriptional profiles assigned to the day of cell retrieval. CD45$^+$CD11b$^+$ cells undergo extensive changes in their transcriptome during retinal engraftment and by day 7 acquire an identical signature to naive microglia. **(B)** Singlec1$^+$ gene is expressed in clusters 3 and 4, both assigned to day 1, suggestive of the presence of monocytes within the microglia sample. **(C)** tSNE analysis of *cx3cr1*, *ccr2*, *p2ry12, tmem119*, *aif1*, and *fcrls* expression in cluster 4 and **(D)** graphical representation of the expression of microglia markers *p2ry12 tmem119, AIF1, and fcrls* in the 4 clusters, including those representatives of microglia and monocytes signatures. **(E)** Flow cytometric analysis of the expression of CD45 marker in retinal CX3CR1$^+$ cells before and 1, 4, and 7 days after injury. A transgenic CX3CR1$^{+/EGFP}$ mouse was used to show the expected CD45 profile of pure microglia from a non-chimera and without injury, while the BMT panels show the evolution in the experimental model. As reference we used a CX3CR1$^{+/EFGP}$ mouse, stained with CD45 markers. Double positive CD45$^+$ CX3CR1$^+$ cells represent only microglia, since naïve eyes do not have infiltration of monocytes[2]. To map infiltrating/engrafting monocytes, we used a CX3CR1$^{+/EGFP}$ bone marrow chimera. CX3CR1$^+$ CD45$^+$ infiltrating monocytes gradually transitioned their CD45 expression towards the expression of naïve microglia at 7 days.

Figure 2. Protein expression of P2RY12, TMEM119 and FCRLS by engrafted monocytes.

(A) CX3CR1$^{+/EGFP}$::CCR2$^{+/RFP}$ bone marrow chimeras were used to differentiate engrafted monocytes from embryonic microglia, followed by immunostaining and flow cytometry to assess expression of P2RY12, TMEM119, and FCRLS proteins. Engrafted monocytes were recognized as EGFP$^+$ RFP$^+$ cells while embryonic microglia were EGFP$^-$ RFP$^-$ cells. **(B)** P2RY12 is not expressed at day 1 and day 7 after monocyte infiltration into the retina, however 55% of EGFP$^+$ engrafted monocytes showed positive expression of P2RY12 at day 45. ***, $P < 0.001$. **(C)** Twenty-five percent of EGFP$^+$ peripheral monocytes (white arrow) expressed TMEM119 at day 1. By day 7, all GFP$^+$ engrafted monocytes are TMEM119$^+$. TMEM119 expression in engrafted monocytes is retained at day 45. (B, C) Data displayed as Mean ± SEM, independent t test **$P < 0.01$; ***$P < 0.001$. Each dot represents 1 animal. Minimum of 3 animals per group. Yellow arrows indicate EGFP$^-$ microglia, white arrows GFP$^+$ engrafted monocytes. *Scare bar = 50 μm.* **(D-E)** A CX3CR1$^{+/EGFP}$::CCR2$^{+/RFP}$ bone marrow chimera was employed to assess FCRLS expression in monocytes and microglia by flow cytometry. BMT CX3CR1$^+$ cells were labeled with a conjugated antibody against CX3CR1 (APC) which allowed differentiation between embryonic microglia (APC$^+$ EGFP$^-$) and engrafted monocytes (APC$^+$ EGFP$^+$). Blood monocytes had no FCRLS expression (grey). One day after infiltration, APC$^+$ EGFP$^+$ peripheral monocytes (purple) acquired strong FCRLS expression, which was comparable to naïve embryonic microglia. FCRLS expression was retained by engrafted monocytes sustained at day 7. At day 45, FCRLS expression was similar to embryonic microglia in the same injured tissue or to naïve microglia. Mean ± SEM, independent t-test,*$P < 0.05$. *Each dot represents 1 anima. Minimum of 3 animals per group. MFI: Median Fluorescence Intensity, Mφ: macrophages, μG: microglia.*

Figure 3. ATAC-seq analysis to assess chromatin accessibility for *p2ry12, fcrls, aif1* (*iba1*), and *tmem119* genes in engrafted monocytes and microglia

In ATAC seq, peak width refers to the horizontal extent of a peak in the ATAC-seq signal track. It represents the range over which chromatin accessibility is elevated. A wider peak indicates a broader region of accessible chromatin. Peak amplitude refers to the height or intensity of the peak in the ATAC-seq signal track. It represents the level of chromatin accessibility at the peak's center. Higher amplitude suggests more frequent chromatin accessibility in that region. In the current study, circulating monocytes and naïve microglia were used as controls. Groups and color coding are listed in engrafted monocytes showed similar open chromatin peaks to circulating monocytes (blue arrows) but also displayed new open chromatin peaks not previously present in circulating monocytes (red arrows) but present in native (embryonic) microglia. One of the peaks under the *p2ry12* gene in naïve microglia (red arrow) was absent in circulating monocytes but acquired upon engraftment into the retina (Fig. 3 B). The *fcrls* gene had similar open chromatin peak across all groups (Fig. 3 C), though naïve microglia had wider and higher peak as compared to circulating monocytes (blue peak compared to grey). After engraftment, the amplitude of this peak increased in monocytes and became similar to microglia at day 45 (blue peak compared to purple), (Fig. 3 C). Similarly, *tmem119* chromatin was not accessible in circulating monocytes, however, it became accessible after monocyte engraftment into the retina (red arrow), (Fig. 3 D). Lastly, AIF1 gene (IBA1) had similar open chromatin peaks among the groups, corroborating the above transcriptional and protein findings showing gain of IBA1 expression by monocytes after engraftment into the retina (Fig. 3 E). **(A)** Color coding of analyzed groups. **(B)** *p2ry12* gene contains 3 open chromatin peaks, 2 of the peaks (blue arrowhead) are similar between the groups, but the 3rd peak is present in microglia (red arrowhead) but not in circulating monocytes. Upon engraftment into the retina, monocytes acquire the 3rd peak (red arrowhead) which is retained throughout the study period (45 days). **(C)** Open chromatin peaks for *fcrls* gene appear similar between the groups, with differences only in the amplitude of the peaks at 45 days in microglia and engrafted monocytes which have higher peaks compared to circulating monocytes or monocytes during early engraftment into the retina (7 days). **(D)** Open chromatin peaks for *aif1* gene (IBA1) appear similar between the groups, although microglia appeared to abolish one peak (red arrowhead) at 7 and 45 days after the injury. **(E)** *tmem119* has only one open chromatin peak, which is present in microglia but not in circulating monocytes, but upon engraftment, peripheral monocytes acquire this distinct peak (red arrowhead). **(F)** Heat map analysis of consensus peaks. Chromatin accessibility is scaled by row (Z-score) to emphasize relative differences across samples. Each row represents a genomic peak, and each column represents a biological replicate. Blood monocyte, n=6; Engrafted Mφ, n=5, including 3 samples of 7 days post injury and 2 samples of 45 days post injury; Naive μG, n=4; Injured μG, n=5, including 2 samples of 7 days post injury and 3 samples of 45 days post injury. The analysis shows engrafted monocytes at day 7 and 45 cluster more closely with microglia than with circulating blood monocytes, visually confirming a shift in the epigenetic landscape. Monocytes undergo significant open chromatin alterations upon engraftment into the retina which enables differentiation from circulating monocytes to tissue-phagocytes. Monocytes increase chromatin accessible for genes *p2ry12*, *tmem119*, *fcrls*, and *aif1* upon engraftment into the retina eventually acquiring a similar open chromatin signature to microglia.

Figure 4. ATAC-seq motif analysis for discovery of putative transcription factors regulating monocyte engraftment.

Motif analysis of differential open chromatin peaks identified by comparing naive microglia, retinal engrafted monocyte (7 and 45 days) compared to circulating monocytes. Blue section contains motifs

assigned to transcription factors previously identified in human and mouse microglia, such as PU.1 (most common), CTCF, IRF, RUNX, MEF2, C/EBP, AP-1, MAF, and MEF. Green section contains enriched motifs assigned to novel transcription factors, such as STAT1, FOXN1, KLFs, ATF3, and Npas4. Red section contains previously reported disease associated motifs, such as MITF and NFKB1. Analysis of naive microglia identifies multiple reported factors but not MAF and MEF, which are identified only in engrafted monocytes. Engrafted monocyte at 7 and 45 days contain highly enriched motifs assigned to the above-mentioned transcription factors CEBP, IRF2, and ATF3. Disease-associated motifs assigned to MITF and NFKB1 are identified in engrafted monocytes but not in microglia. *E-value <0.05 for statistically significant motifs*.

Figure 5. Expression of conventional markers by microglia and engrafted monocytes.
(A) Development of a CX3CR1$^{+/EGFP}$::CCR2$^{+/RFP}$ bone marrow chimera model to differentiate microglia from peripheral monocytes following flow cytometry. Microglia: EGFP^{-} CX3CR1-APC^{+}, engrafted monocytes: EGFP^{+}CX3CR1-APC^{+}. **(B)** Peripheral monocyte/macrophages repress CCR2 expression and enhance CX3CR1 expression during engraftment into the retina. Five distinct maturation phases of monocytes after engraftment are identified (Groups 1-5). A separate group of CCR^{-}CX3CR1^{-} cells, representing embryonic microglia (Group 6; µG), is retained throughout the study period (45 days). **(C-D)** Engrafted monocytes have increase expression of Ly6C at day 1 of infiltration, which is gradually suppressed during engraftment. At 45 days, the majority of engrafted monocytes (Group 5) have similar Ly6G expression as microglia (Group 6). *ns*, not significant, independent t test, ****P < 0.001*. Each dot represents 1 animal. Minimum of 8 animals per group. **(E-F)** Engrafted monocytes exhibit sustained expression of CD45 at days 1 and 7 followed by repression in subpopulations of these cells (Group 5), and at day 45 reaching equal levels compared to retinal microglia (Group 6). Independent t test, **P < 0.01, ***P < 0.001. Each dot represents 1 animal. Minimum of 8 animals per group. **(G)** A clear population of CD45^{high} and CD45^{int} is present at day 1 and 7 after injury, but not at day 45 due to CD45 repression in engrafted monocytes.

Figure 6. Summary of the microglia and monocyte signature
Monocyte transition from highly amoeboid to highly ramified cells during engraftment into the retina, becoming morphometrically identical and indistinguishable from retinal microglia. These changes are accompanied by suppression of monocyte markers CCR2, Ly6C, and CD45, and upregulation of the tissue-resident macrophage marker CX3CR1$^{+/GFP}$ and microglia markers IBA1, TMEM119, P2RY12, and FCRLS. P2RY12 appears to be conditionally specific to microglia during early infiltration of monocytes) and to a subpopulation of engrafted monocytes.

Sup. Figure S1. Efficiency of CX3CR1$^{+/EGFP}$::CCR2$^{+/RFP}$ bone marrow chimerism with busulfan.
(A) Chimerism efficiency was assessed 30 days after cell transplantation in busulfan myelodepleted mice. **(B)** 95% of the blood CD45^{+}CD11b^{+}CX3CR1^{+} cells were EGFP^{+}/RFP^{+} donor cells suggesting a chimerism efficiency of ~95% (n= 4 mice). **(C)** Representation of the gating strategy to differentiate host vs donor CX3CR1^{+} blood cells.

Sup. Figure S2. mRNA expression of *p2ry12*, *tmem119*, *fcrls*, and *aif1* (*iba1* gene) in blood monocytes, embryonic retinal microglia, and engrafted retinal monocytes.

A CX3CR1$^{+/GFP}$ bone marrow chimera model was employed to differentiate peripheral infiltrating monocytes from embryonic retinal microglia according to the following gating strategy: CD45^{+}CD11b^{+} CX3CR1-EGFP^{-}CX3CR1^{-}BV605^{+} for microglia, CD45^{+}CD11b^{+} CX3CR-EGFP^{+}CX3CR1^{-}BV605^{+} for blood or tissue engrafted monocytes. Uninjured chimeras were used as controls for naïve microglia and naïve blood monocytes. Microglia and tissue engrafted monocytes were collected from retinas, 45 days after corneal alkali injury. *p2ry12*, *tmem119*, *fcrls* and *iba1 m*RNA expression was assessed in isolated cells using real-time qPCR. *P2ry12*, *tmem119*, and *iba1* mRNA levels were normalized to blood monocytes. *fcrls* mRNA expression was normalized based on the expression in naïve retinal microglia, due to lack of expression in blood monocytes. *p2ry12*, *tmem119*, *fcrls*, and *iba1* mRNA expression in monocytes increased after engraftment into the retina. Each dot indicates 1 animal, n≥3 mice per analysis.

Sup. Figure S3. Circulating monocytes do not express microglia makers.
Immunostaining of circulating blood monocytes from CX3CR1$^{+/EGFP}$::CCR2$^{+/RFP}$ transgenic mice shows absence of P2RY12, IBA1, and TMEM119 protein expression in blood monocytes. Some circulating monocytes are either CCR2 or CX3CR1 positive with some expressing both markers simultaneously. However, MHC-II expression was predominantly expressed in circulating monocytes regardless of their CCR2 or CX3CR1 expression. Scare bar = 20 µm

Sup. Figure S4. P2RY12 expression in engrafted monocyte at 14 days.
Flat mount confocal microscopy of retinas from CX3CR1$^{+/EGFP}$::CCR2$^{+/RFP}$ bone marrow chimeras. Engrafted monocytes are labeled as EGFP^{+}CCR2^{+} and embryonic microglia as EGFP^{-} CCR2^{-}. P2RY12 is expressed in peripheral monocytes 14 days after engraftment into the retina. P2RY12^{+} engrafted monocytes abolish CCR2 expression. *Scale bar = 50 µm*.

Sup. Figure S5. Long-term expression of P2RY12, TMEM119 and IBA1 in monocytes 16 month after retinal engraftment.
(A) Fate mapping of engrafted monocytes and embryonic microglia using a bone marrow chimera model. Wild-type mice were myelodepleted with busulfan and transplanted with donor bone marrow cells from CX3CR1$^{CreER-EYFP}$::ROSA26^{tdTomato} mice. An ocular injury was performed after chimerism, followed by tamoxifen treatment 2 weeks later. Mice were followed for 16 months, and retinal cells were analyzed. **(B)** YFP^{+} tdTomato^{+} engrafted monocytes continued to have expression of P2RY12 16 months after infiltration. **(C)** Likewise, YFP^{+} tdTomato^{+} engrafted monocytes retained expression of TMEM119 and (**D)** IBA1 16 months after injury. n=3. *Scare bar = 20 µm. BMT: Bone marrow transplant; TAM: Tamoxifen; w: week; m: months. Monocytes (white arrows): YFP^{+} tdTomato^{+}, Microglia (Yellow arrows): YFP^{-neg} tdTomato^{-neg}.*

Sup. Figure S6. **Flow cytometric strategy to differentiate monocytes from microglia.**
(A) Experimental timeline of the bone marrow chimeras for the differentiation of engrafted monocytes from embryonic microglia. **(B)** Flow cytometry gating strategy for differentiation of embryonic microglia from engrafted monocytes in the bone marrow chimeras. Cells are sorted based on their forward (FSC) and side (SSC) scattering and then subjected to single-cell gating (FSC-A and FSC-H) for live cells separation (DAPI^{-}). Immune cells are labeled as CD11b^{+}CD45^{+} with embryonic microglia being

classified as CX3CR1^{-}PE-Cy7^{+} CX3CR1-EGFP^{-} and engrafted monocytes as CX3CR1^{-}PE-Cy7^{+} CX3CR1-EGFP^{+}.

Sup. Figure S7. Protein expression of IBA1 in engrafted monocytes.
The CX3CR1$^{+/GFP}$::CCR2$^{+/RFP}$ bone marrow chimeras were employed to differentiate engrafted monocytes from embryonic microglia. Eighty-five percent of engrafted EGFP^{+} monocytes were shown to express IBA1^{+} at 1 day after infiltration, while 100% of the infiltrated cells expressed IBA1^{+} at day 7 or day 45 of engraftment. *ns: Not significant. Yellow arrows indicate EGFP$^{-negative}$ IBA1$^{+positive}$ microglia cells and white arrows EGFP$^{+positive}$ engrafted monocytes. Scare bar = 50 µm. ns: non-significant, independent t-test. Each dot represents 1 animal. Minimum of 3 animals per group*.

Sup. Figure S8. Protein expression of P2RY12, TMEM119 and IBA1 by engrafted monocytes in mouse retina after NaIO3 RPE injury.
(A) CX3CR1$^{+/GFP}$ bone marrow transplant model was used to differentiate engrafted monocytes from embryonic microglia. Monocytes (white arrows) are EGFP^{+} while Microglia are EGFP^{-} **(B)** TMEM119, IBA1, P2RY12 and MHC II expression in EGFP^{+} engrafted monocytes 14 days after NaIO3 induced RPE injury. n=1. *Scare bar = 50 µm* **(C)** TMEM119, IBA1, P2RY12 and MHC II expression in EGFP^{+} engrafted monocytes 3 months after NaIO3 induced RPE injury. MHC II staining as staining control. n=4. *Scare bar = 20 µm.*

Sup. Figure S9. Protein expression of P2RY12, TMEM119, IBA1 and MHC II by engrafted monocytes in young mouse brain and spinal cord without injury.
(A) CX3CR1$^{+/GFP}$ bone marrow transplant model was used to differentiate engrafted monocytes from embryonic microglia. One month after bone marrow translation, brain and spinal cord was collected. Monocytes (white arrows) are EGFP^{+} while Microglia are EGFP^{-}. **(B)** In brain, IBA1, TMEM119 was expressed in all EGFP^{+} engrafted monocytes, while P2RY12 was weekly expressed in 50% of EGFP^{+} engrafted monocytes and MHC II expression was not detected. **(C)** In spinal cord, IBA1, TMEM119 was expressed in all EGFP^{+} engrafted monocytes, while P2RY12 and MHC II expression was not detected. n=3. *Scare bar = 50 µm. Monocytes (white arrows):* EGFP^{++}*, Microglia (Yellow arrows):* EGFP^{-}.

Sup. Figure S10. Protein expression of P2RY12, TMEM119, IBA1 and MHC II by engrafted monocytes in aged mouse brain and spinal cord without injury.
(A) CX3CR1$^{+/GFP}$ bone marrow transplant model was used to differentiate engrafted monocytes from embryonic microglia. One year after bone marrow translation, brain and spinal cord was collected. Monocytes (white arrows) are EGFP^{+} while Microglia are EGFP^{-}. **(B)** In brain, IBA1, TMEM119 and P2RY12 was expressed in all EGFP^{+} engrafted monocytes, while MHC II expression was not detected. **(C)** In spinal cord, IBA1, TMEM119 and P2RY12 was expressed in all EGFP^{+} engrafted monocytes, while MHC II expression was not detected. n=3. *Scare bar = 50 µm. Monocytes (white arrows):* EGFP^{++}*, Microglia (Yellow arrows):* EGFP^{-}.

Table 1. Antibody information for flow Cytometry and immunostaining.
Both P2RY12 antibodies worked successfully in our experimental investigations.

Data Availability Statemen

The data supporting the findings of this article are available within the article and/or its supplementary materials.

Bibliography

1. Kamimura, D., et al., *The gateway theory: bridging neural and immune interactions in the CNS.* Front Neurosci, 2013. **7**: p. 204.
2. Paschalis, E.I., et al., *Permanent neuroglial remodeling of the retina following infiltration of CSF1R inhibition-resistant peripheral monocytes.* Proc Natl Acad Sci U S A, 2018. **115**(48): p. E11359-e11368.
3. Paschalis, E.I., et al., *The Role of Microglia and Peripheral Monocytes in Retinal Damage after Corneal Chemical Injury.* Am J Pathol, 2018. **188**(7): p. 1580-1596.
4. Paschalis, E.I., et al., *Microglia Regulate Neuroglia Remodeling in Various Ocular and Retinal Injuries.* J Immunol, 2019. **202**(2): p. 539-549.
5. Spiteri, A.G., et al., *Microglia and monocytes in inflammatory CNS disease: integrating phenotype and function.* Acta Neuropathol, 2022. **143**(2): p. 179-224.
6. Bennett, M.L., et al., *New tools for studying microglia in the mouse and human CNS.* Proc Natl Acad Sci U S A, 2016. **113**(12): p. E1738-46.
7. Butovsky, O., et al., *Identification of a unique TGF-β-dependent molecular and functional signature in microglia.* Nat Neurosci, 2014. **17**(1): p. 131-43.
8. Ronning, K.E., S.J. Karlen, and M.E. Burns, *Structural and functional distinctions of co-resident microglia and monocyte-derived macrophages after retinal degeneration.* J Neuroinflammation, 2022. **19**(1): p. 299.
9. Paschalis, E.I., et al., *Mechanisms of Retinal Damage after Ocular Alkali Burns.* Am J Pathol, 2017. **187**(6): p. 1327-1342.
10. Saban, D.R., *New concepts in macrophage ontogeny in the adult neural retina.* Cell Immunol, 2018. **330**: p. 79-85.
11. Kim, H.J., et al., *Blood monocyte-derived CD169(+) macrophages contribute to antitumor immunity against glioblastoma.* Nat Commun, 2022. **13**(1): p. 6211.
12. Lei, F., et al., *CSF1R inhibition by a small-molecule inhibitor is not microglia specific; affecting hematopoiesis and the function of macrophages.* Proc Natl Acad Sci U S A, 2020. **117**(38): p. 23336-23338.
13. Ma, W., et al., *Human-induced pluripotent stem cell-derived microglia integrate into mouse retina and recapitulate features of endogenous microglia.* Elife, 2024. **12**.
14. Saeed, S., et al., *Epigenetic programming of monocyte-to-macrophage differentiation and trained innate immunity.* Science, 2014. **345**(6204): p. 1251086.
15. Gibbings, S.L., et al., *Transcriptome analysis highlights the conserved difference between embryonic and postnatal-derived alveolar macrophages.* Blood, 2015. **126**(11): p. 1357-66.
16. van de Laar, L., et al., *Yolk Sac Macrophages, Fetal Liver, and Adult Monocytes Can Colonize an Empty Niche and Develop into Functional Tissue-Resident Macrophages.* Immunity, 2016. **44**(4): p. 755-68.
17. Gosselin, D., et al., *An environment-dependent transcriptional network specifies human microglia identity.* Science, 2017. **356**(6344).

638 18. Dolan, M.J., et al., *Exposure of iPSC-derived human microglia to brain substrates enables the*
639 *generation and manipulation of diverse transcriptional states in vitro.* Nat Immunol, 2023. **24**(8): p.
640 1382-1390.
641 19. King, I.L., T.L. Dickendesher, and B.M. Segal, *Circulating Ly-6C+ myeloid precursors migrate to*
642 *the CNS and play a pathogenic role during autoimmune demyelinating disease.* Blood, 2009.
643 **113**(14): p. 3190-7.
644 20. Martin, E., et al., *Analysis of Microglia and Monocyte-derived Macrophages from the Central*
645 *Nervous System by Flow Cytometry.* J Vis Exp, 2017(124).
646 21. Wolf, S.A., H.W. Boddeke, and H. Kettenmann, *Microglia in Physiology and Disease.* Annu Rev
647 Physiol, 2017. **79**: p. 619-643.
648 22. Benmamar-Badel, A., T. Owens, and A. Wlodarczyk, *Protective Microglial Subset in Development,*
649 *Aging, and Disease: Lessons From Transcriptomic Studies.* Front Immunol, 2020. **11**: p. 430.
650 23. Zeng, J., et al., *The mechanism of microglia-mediated immune inflammation in ischemic stroke and*
651 *the role of natural botanical components in regulating microglia: A review.* Front Immunol, 2022. **13**:
652 p. 1047550.
653 24. Choi, I., et al., *Autophagy enables microglia to engage amyloid plaques and prevents microglial*
654 *senescence.* Nat Cell Biol, 2023. **25**(7): p. 963-974.
655 25. Lv, Q.K., et al., *Role of alpha-synuclein in microglia: autophagy and phagocytosis balance*
656 *neuroinflammation in Parkinson's disease.* Inflamm Res, 2023. **72**(3): p. 443-462.
657 26. Zhou, C., et al., *Sustained Inhibition of VEGF and TNF-α Achieves Multi-Ocular Protection and*
658 *Prevents Formation of Blood Vessels after Severe Ocular Trauma.* Pharmaceutics, 2023. **15**(8).
659 27. Kenkhuis, B., et al., *Co-expression patterns of microglia markers Iba1, TMEM119 and P2RY12 in*
660 *Alzheimer's disease.* Neurobiol Dis, 2022. **167**: p. 105684.
661 28. Sideris-Lampretsas, G., et al., *Galectin-3 activates spinal microglia to induce inflammatory*
662 *nociception in wild type but not in mice modelling Alzheimer's disease.* Nat Commun, 2023. **14**(1): p.
663 3579.
664 29. Matek, W., et al., *Initial experience with the new electronic endoscope.* Endoscopy, 1984. **16**(1): p.
665 20-1.
666 30. Haimon, Z., et al., *Cognate microglia-T cell interactions shape the functional regulatory T cell pool*
667 *in experimental autoimmune encephalomyelitis pathology.* Nat Immunol, 2022. **23**(12): p. 1749-1762.
668 31. Vankriekelsvenne, E., et al., *Transmembrane protein 119 is neither a specific nor a reliable marker*
669 *for microglia.* Glia, 2022. **70**(6): p. 1170-1190.
670 32. Stratoulias, V., et al., *ARG1-expressing microglia show a distinct molecular signature and modulate*
671 *postnatal development and function of the mouse brain.* Nat Neurosci, 2023. **26**(6): p. 1008-1020.
672 33. Wu, Q., et al., *Microglial activation and over pruning involved in developmental epilepsy.* J
673 Neuropathol Exp Neurol, 2023. **82**(2): p. 150-159.
674 34. Yin, Z., et al., *Identification of a protective microglial state mediated by miR-155 and interferon-*
675 *gamma signaling in a mouse model of Alzheimer's disease.* Nat Neurosci, 2023. **26**(7): p. 1196-1207.
676 35. Chen, X., et al., *Microglia-mediated T cell infiltration drives neurodegeneration in tauopathy.* Nature,
677 2023. **615**(7953): p. 668-677.
678 36. O'Koren, E.G., R. Mathew, and D.R. Saban, *Fate mapping reveals that microglia and recruited*
679 *monocyte-derived macrophages are definitively distinguishable by phenotype in the retina.* Sci Rep,
680 2016. **6**: p. 20636.
681 37. Zhou, N., et al., *Transcriptional mechanism of IRF8 and PU.1 governs microglial activation in*
682 *neurodegenerative condition.* Protein Cell, 2019. **10**(2): p. 87-103.

683 38. Hammond, T.R., et al., *Single-Cell RNA Sequencing of Microglia throughout the Mouse Lifespan and*
684 *in the Injured Brain Reveals Complex Cell-State Changes.* Immunity, 2019. **50**(1): p. 253-271.e6.
685 39. Kierdorf, K., et al., *Bone marrow cell recruitment to the brain in the absence of irradiation or*
686 *parabiosis bias.* PLoS One, 2013. **8**(3): p. e58544.
687 40. Huang, Y., et al., *Dual extra-retinal origins of microglia in the model of retinal microglia*
688 *repopulation.* Cell Discov, 2018. **4**: p. 9.
689 41. Skene, P.J., J.G. Henikoff, and S. Henikoff, *Targeted in situ genome-wide profiling with high*
690 *efficiency for low cell numbers.* Nat Protoc, 2018. **13**(5): p. 1006-1019.
691 42. O'Koren, E.G., et al., *Microglial Function Is Distinct in Different Anatomical Locations during*
692 *Retinal Homeostasis and Degeneration.* Immunity, 2019. **50**(3): p. 723-737.e7.
693 43. Li, H. and R. Durbin, *Fast and accurate short read alignment with Burrows-Wheeler transform.*
694 Bioinformatics, 2009. **25**(14): p. 1754-60.
695 44. John, S., et al., *Chromatin accessibility pre-determines glucocorticoid receptor binding patterns.* Nat
696 Genet, 2011. **43**(3): p. 264-8.
697

Figure 1

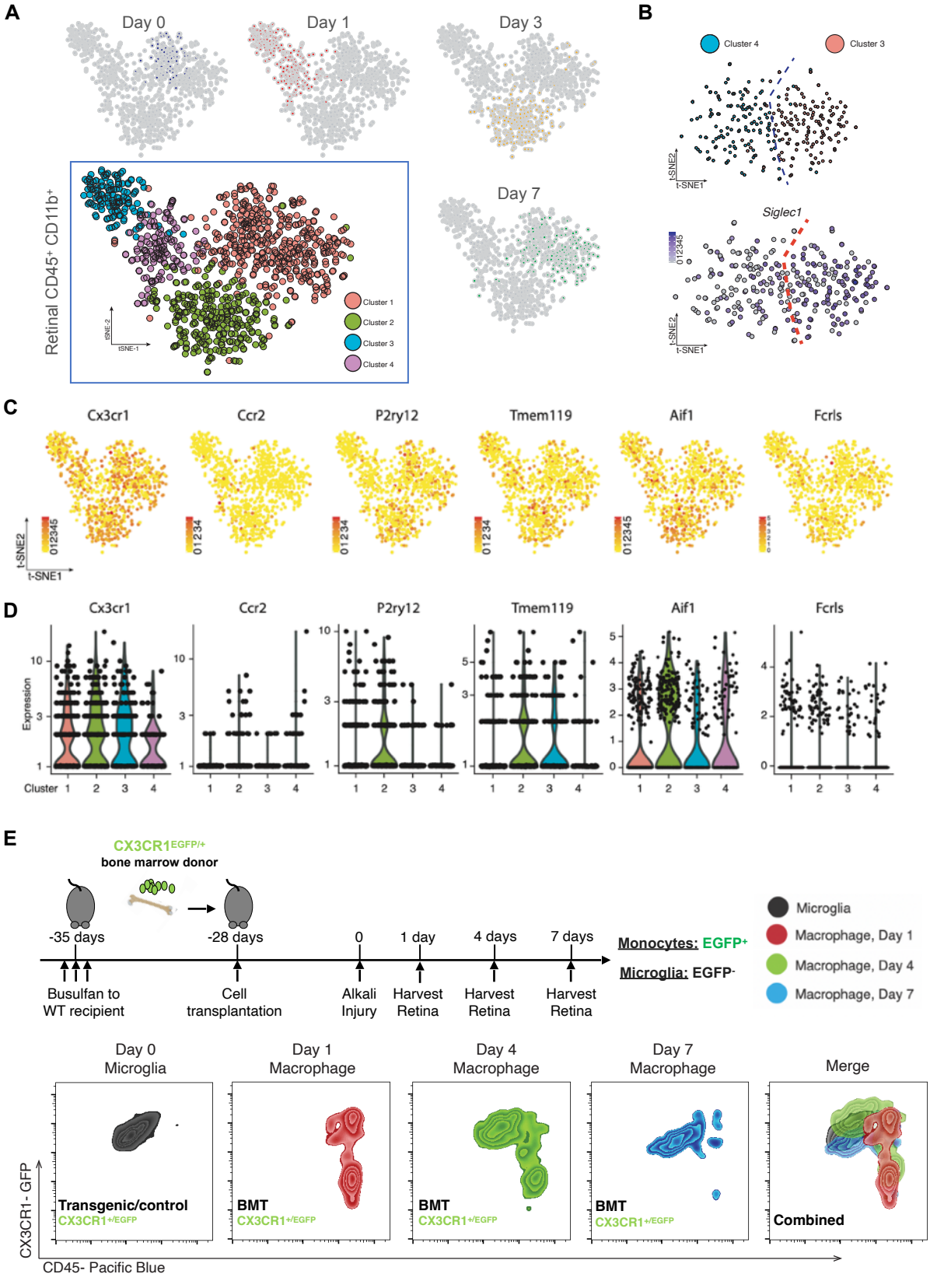
A
Day 0
Day 1
Day 3
Day 7
Retinal CD45+ CD11b+
tSNE-2
tSNE-1
Cluster 1
Cluster 2
Cluster 3
Cluster 4
B
Cluster 4
Cluster 3
t-SNE2
t-SNE1
Siglec1
012345
C
Cx3cr1
Ccr2
P2ry12
Tmem119
Aif1
Fcrls
D
Expression
Cluster
E
CX3CR1EGFP/+
bone marrow donor
-35 days
-28 days
0
1 day
4 days
7 days
Busulfan to WT recipient
Cell transplantation
Alkali Injury
Harvest Retina
Monocytes: EGFP+
Microglia: EGFP-
Microglia
Macrophage, Day 1
Macrophage, Day 4
Macrophage, Day 7
Day 0 Microglia
Day 1 Macrophage
Day 4 Macrophage
Day 7 Macrophage
Merge
Transgenic/control
CX3CR1+/EGFP
BMT
CX3CR1+/EGFP
Combined
CX3CR1- GFP
CD45- Pacific Blue

Figure 2

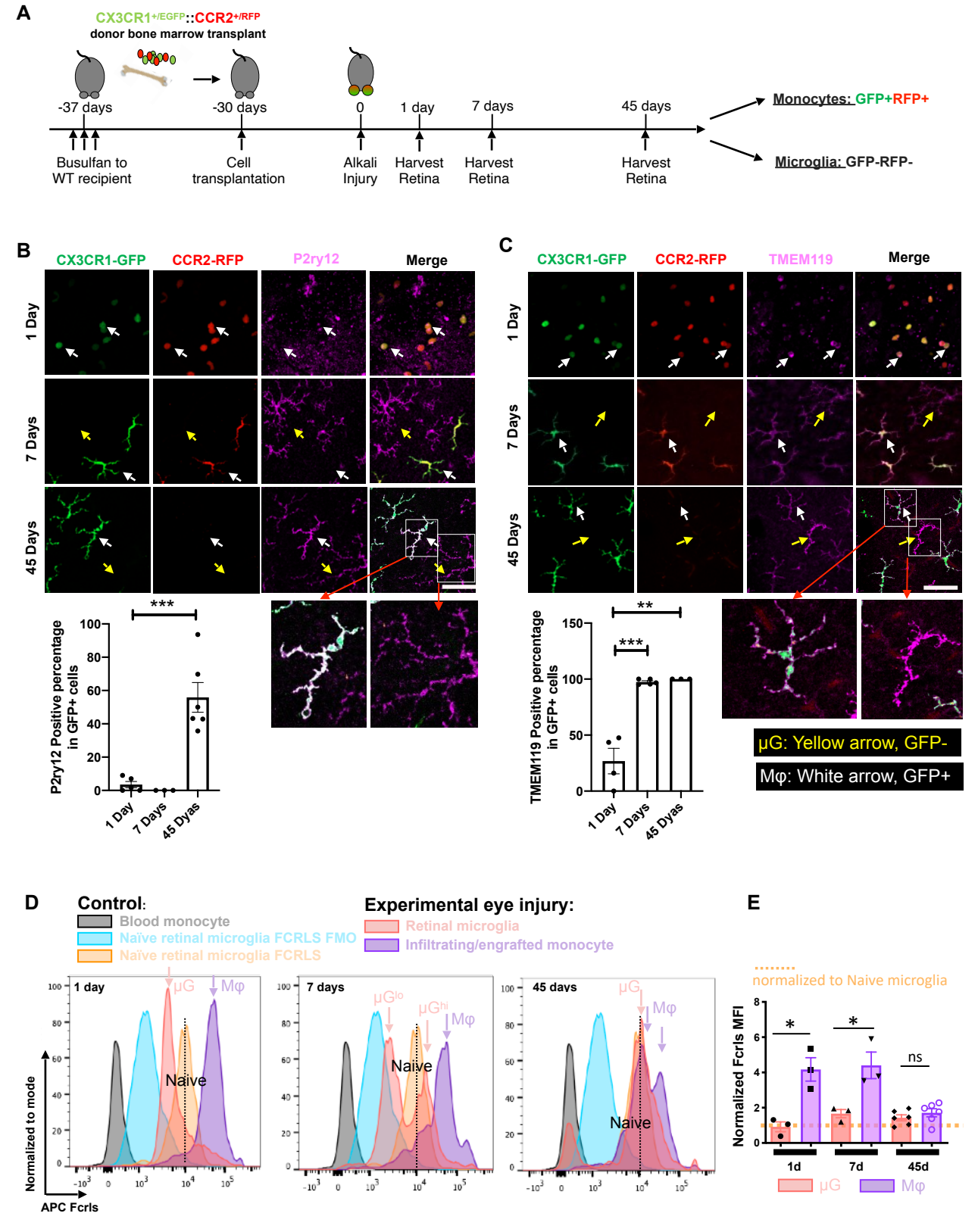
A
CX3CR1+/EGFP::CCR2+/RFP
donor bone marrow transplant
-37 days
-30 days
0
1 day
7 days
45 days
Busulfan to WT recipient
Cell transplantation
Alkali Injury
Harvest Retina
Harvest Retina
Harvest Retina
Monocytes: GFP+RFP+
Microglia: GFP-RFP-
B
CX3CR1-GFP
CCR2-RFP
P2ry12
Merge
1 Day
7 Days
45 Days
P2ry12 Positive percentage in GFP+ cells
***
1 Day
7 Days
45 Dyas
C
CX3CR1-GFP
CCR2-RFP
TMEM119
Merge
TMEM119 Positive percentage in GFP+ cells
**
***
μG: Yellow arrow, GFP-
Mφ: White arrow, GFP+
D
Control:
Blood monocyte
Naïve retinal microglia FCRLS FMO
Naïve retinal microglia FCRLS
Experimental eye injury:
Retinal microglia
Infiltrating/engrafted monocyte
1 day
7 days
45 days
μG
Mφ
μGlo
μGhi
Naive
Normalized to mode
APC Fcrls
E
normalized to Naive microglia
Normalized Fcrls MFI
*
ns
1d
7d
45d
μG
Mφ

Figure 3

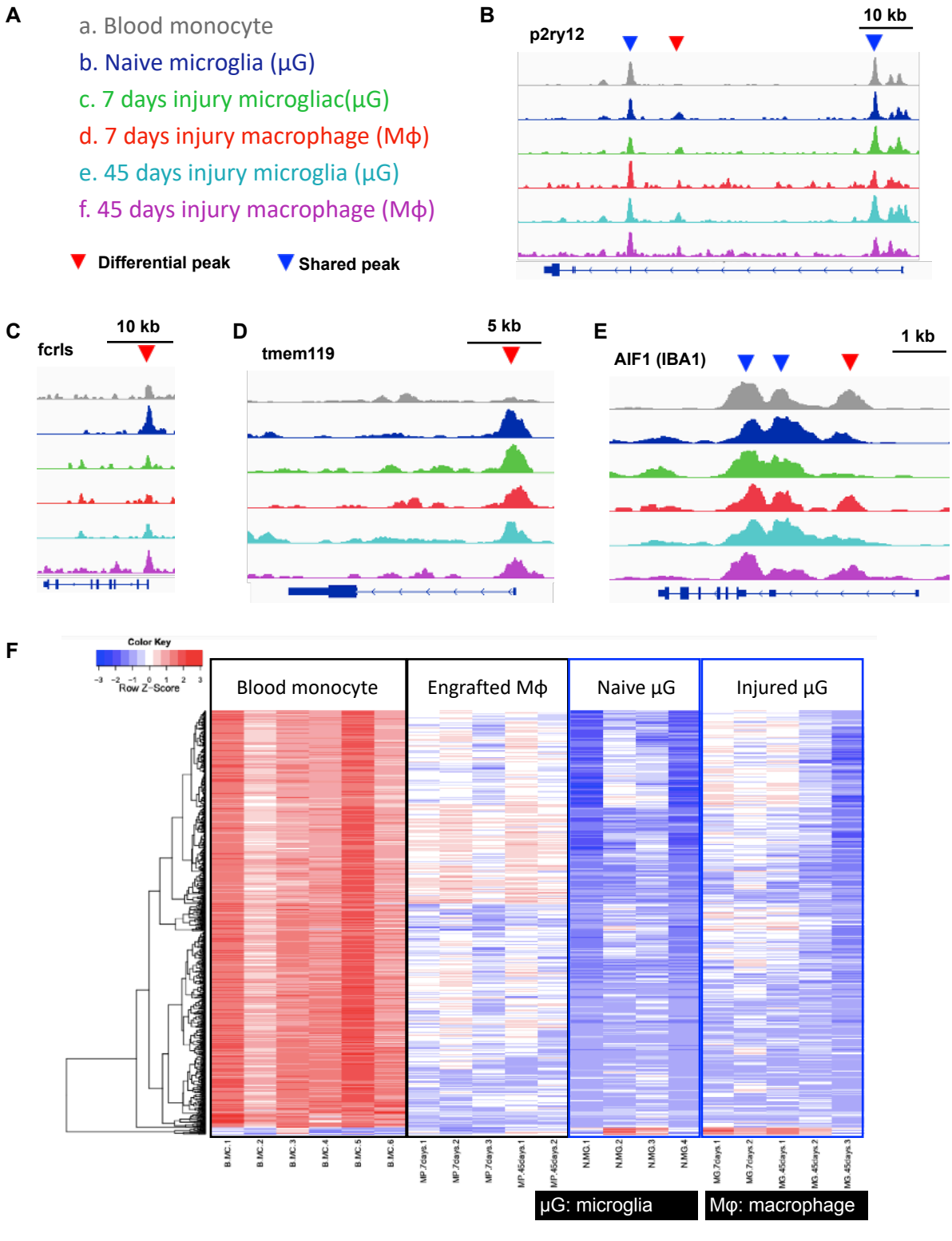
A
a. Blood monocyte
b. Naive microglia (μG)
c. 7 days injury microgliac(μG)
d. 7 days injury macrophage (Mϕ)
e. 45 days injury microglia (μG)
f. 45 days injury macrophage (Mϕ)
Differential peak
Shared peak
B
p2ry12
10 kb
C
fcrls
10 kb
D
tmem119
5 kb
E
AIF1 (IBA1)
1 kb
F
Color Key
Row Z-Score
Blood monocyte
Engrafted Mϕ
Naive μG
Injured μG
B.MC.1
B.MC.2
B.MC.3
B.MC.4
B.MC.5
B.MC.6
MP.7days.1
MP.7days.2
MP.7days.3
MP.45days.1
MP.45days.2
N.MG.1
N.MG.2
N.MG.3
N.MG.4
MG.7days.1
MG.7days.2
MG.45days.1
MG.45days.2
MG.45days.3
μG: microglia
Mϕ: macrophage

Figure 4

(comparing μG/ 7days Mφ/45 days Mφ to blood monocyte)

Motif	Best Match	Naive μG	7 day Mφ	45 day Mφ	
	PU.1	+	+	+	Corroborate previous identified microglia motif
	CTCF	+	-	+	
	RUNX	+	+	-	
	AP-1	+	+	+	
	CEBP	+	-	-	
	IRF2	+	-	-	
	MAF	-	+	+	
	MEF	-	+	-	
	STAT1	+	+	+	Newly identified motif
	FOXN1	+	-	+	
	KLF5/9	+	+	-	
	Atf3	+	-	-	
	Npas4	+	+	-	
	MITF	-	+	+	Disease associated motif
	NFKB1	-	+	-	

Significant Motifs (E-values ≤ 0.05)

μG: microglia
Mφ: macrophage

Figure 5

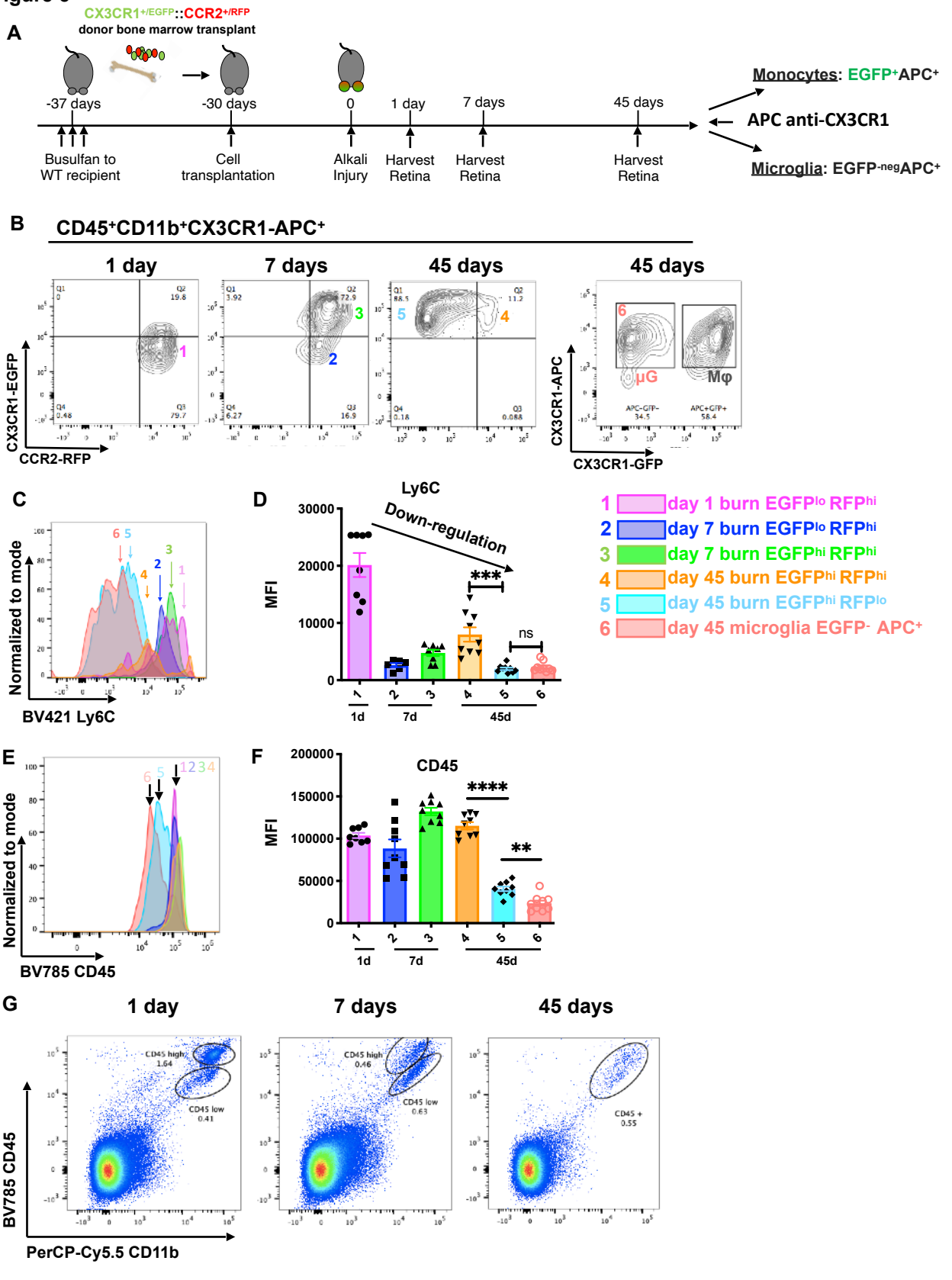
A
CX3CR1+/EGFP::CCR2+/RFP
donor bone marrow transplant
-37 days
-30 days
0
1 day
7 days
45 days
Busulfan to WT recipient
Cell transplantation
Alkali Injury
Harvest Retina
Harvest Retina
Harvest Retina
Monocytes: EGFP+APC+
APC anti-CX3CR1
Microglia: EGFP-negAPC+
B
CD45+CD11b+CX3CR1-APC+
1 day
7 days
45 days
45 days
CX3CR1-EGFP
CCR2-RFP
CX3CR1-APC
CX3CR1-GFP
μG
Mφ
C
Normalized to mode
BV421 Ly6C
D
Ly6C
Down-regulation
MFI
***
ns
1d
7d
45d
1 day 1 burn EGFPlo RFPhi
2 day 7 burn EGFPlo RFPhi
3 day 7 burn EGFPhi RFPhi
4 day 45 burn EGFPhi RFPhi
5 day 45 burn EGFPhi RFPlo
6 day 45 microglia EGFP- APC+
E
Normalized to mode
BV785 CD45
F
CD45
MFI
****
**
1d
7d
45d
G
1 day
7 days
45 days
CD45 high 1.64
CD45 low 0.41
CD45 high 0.46
CD45 low 0.63
CD45 + 0.55
BV785 CD45
PerCP-Cy5.5 CD11b

Figure 6

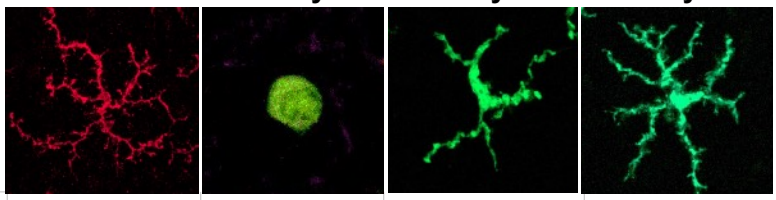

	YS µG	Engrafted Mφ		
		1 day	7 days	45 days
Cell-type	**YS µG** Ramified/ small soma	**Mφ** Ameboid/ large soma	**Mφ** Semi-ramified/ large soma	**Mφ** Ramified/ large soma
IBA1	**+**	**+**	**+**	**+**
TMEM119	**+**	**Lo**	**+**	**+**
P2ry12	**+**	**-**	**-**	**Lo/Hi***
Fcrls	**+**	**Hi**	**Hi**	**+/Hi**
CCR2	-	Hi	Low	-
CX3CR1	+	Lo	Lo/Hi*	Hi
Ly6C	-	Hi	Hi	-/Lo*
CD45	Int	Hi	Hi	Int/Hi *

**** Heterogeneous***